



Article

A Methodology for Shipping Noise Field Calibration and Excess Noise Estimation: The Azores Case Study

Sérgio M. Jesus ^{1,*}, Cristiano Soares ², Miriam Romagosa ³ , Irma Cascão ³ , Ricardo Duarte ¹, Friedrich Zabel ² and Mónica A. Silva ³ 

¹ Laboratory of Robotics and Engineering Systems (LARSyS), University of Algarve, 8005-139 Faro, Portugal

² Marsensing Lda. Centro Empresarial Pav.A5, Campus de Gambelas, 8005-139 Faro, Portugal

³ Institute of Marine Research-IMAR & Institute of Marine Sciences-Okeanos, University of the Azores, 9901-862 Horta, Portugal

* Correspondence: sjesus@ualg.pt; Tel.: +351-289-800-949

Abstract: Economic globalization and the continuous search for food, energy and raw materials led to an estimated 3 dB/decade increase of ocean noise intensity. Determining the level of anthropogenic noise, the so-called excess noise, and building identifiable meaningful indicators for supporting marine management policies currently requires extensive observation data and computer modeling. For modeling purposes, in this study, anthropogenic noise was reduced to shipping traffic drawn from Automatic Identification System data, and environmental sound was attributed to surface wind only. Data-model comparison allowed introducing a methodology for simple model calibration and estimate excess noise. This methodology was tested on acoustic recordings performed in June 2018 at three locations to the southwest of Faial-Pico Islands in the Azores archipelago. The results show that field-calibrated excess noise sound maps are in line with the shipping distribution in the area, revealing a number of potentially marine life-threatening hotspots. Excess noise addresses the need for a quantifiable measure of ocean noise only and therefore offers a basis for building suitable continuous anthropogenic noise pollution indicators.

Keywords: ocean soundscape; shipping noise; excess noise; field calibration; Azores archipelago



Citation: Jesus, S.M.; Soares, C.; Romagosa M.; Cascão I.; Duarte R.; Zabel F.; Silva M.A. A Methodology for Shipping Noise Field Calibration and Excess Noise Estimation: The Azores Case Study. *J. Mar. Sci. Eng.* **2022**, *10*, 1763. <https://doi.org/10.3390/jmse10111763>

Academic Editor: Claudio Testa, Aristides Prospathopoulos and Luca Greco

Received: 18 October 2022

Accepted: 11 November 2022

Published: 16 November 2022

Publisher's Note: MDPI stays neutral with regard to jurisdictional claims in published maps and institutional affiliations.



Copyright: © 2022 by the authors. Licensee MDPI, Basel, Switzerland. This article is an open access article distributed under the terms and conditions of the Creative Commons Attribution (CC BY) license (<https://creativecommons.org/licenses/by/4.0/>).

1. Introduction

Ambient sound is the acoustic resident field in the ocean and therefore a meaningful tool for long-term environmental monitoring [1]. Ocean soundscaping, or the *art* of determining the interaction of sound with the oceanscape, became a field of intense scientific interest with the long-term promise of inferring the impact of ocean noise on the status of marine life and biodiversity [2–6].

The early work in ocean ambient noise may be summarized by that of Knudsen et al. [7] (1948), Urlick and Price [8] (1954), and culminating with the landmark paper of Wenz [9] (1962), with its picture of power density spectrum under various ocean conditions.

In a classical terminology proposed by Urlick and Price [8], and now somehow outdated, the term “background ambient noise” was coined to designate all the non-informative signal present in a sound recording, reverberation excluded. In most cases, a signal was injected underwater by human activity and noise was all the rest. In the last two or three decades, with the advent and widespread of passive acoustic monitoring, this background noise concept has shifted from human to marine life centered. In that paradigm, which will be used throughout, the generic term “ocean sound” will designate any underwater acoustic vibration; the term “natural sound” will encompass both sound generated by environmental elements, such as wind, waves, ice, rain, earthquakes, etc., as well as the sound of biological origin; and the term “ocean noise” will be reserved for that part of ocean sound that is harmful to marine species (see details in [10]). Since ocean noise

will be almost exclusively due to human activity, the term anthropogenic noise will be used interchangeably with ocean noise.

For many years, the focus of ambient noise studies was on noise structure, i.e., its spatial correlation and directivity. Nowadays, the focus is more on the “amount” of ocean sound, which is classically defined as the sound pressure level (SPL), evaluated in a space-time-frequency grid—a process sometimes known as sound mapping. Sound mapping offers a pictorial cue of sound-level distribution in space and time, with the objective of determining stress locations, with possible impacts on marine species, and to support marine policies for biodiversity protection and conservation. Recently, ocean sound was declared as an essential ocean variable¹ and an additional chapter of the recently published United Nations World Ocean Assessment report was dedicated to ocean noise inputs [11].

A common approximation for sound mapping in the low end frequency band assumes ship traffic as the dominant source of noise and surface wind as the main environmental sound component. Both components may be modeled thanks to database-drawn environmental information, such as bathymetry, ocean temperature and wind speed estimates, and to the availability of Automatic Identification System (AIS) data providing ship type and positioning. Acoustic propagation models have been used for obtaining three-dimensional deterministic representations of the shipping noise field [12–14]. Since this process is very computer intensive, especially for large bathymetrically challenging areas with intense traffic, an alternative would be to represent ship location with a statistical distribution, and therefore, the output ocean noise map becomes also a stochastic process [15]. Sound generated at the sea surface by the action of wind is known to be predominant above a frequency of a few hundred Hz [7,9,16]. Below that frequency, wind sound exists but is exceeded by the noise from distant shipping (30–150 Hz) and earthquakes (<30 Hz). The contribution of Cato [17] with ocean sound surveys in Australian waters where shipping noise is low, and later by Burgess and Kewley [18] using a surface steered vertical array to exclude shipping noise from distant sources, was determinant for establishing an empirical dependence of ocean sound on frequency and wind speed [18,19].

Sound maps suffer from inherent model uncertainties, which call for adjustment with actual field data, which is a process also known as “field calibration”. Field calibration of sound maps has been attempted with various approaches, such as for example by adjusting source level, as proposed in a simulation exercise in [20], or by adjusting bottom parameters in the acoustic models [21]. It remains unclear how to validate the improvement obtained by each field calibration strategy and how this improvement extends for time periods and locations where there are no ground truth observations.

Marine life protection and conservation requires commonly agreed policies, which in turn calls for identifiable and meaningful indicators. For indicator building, it is common practice to separately consider the effects of impulsive noise and continuous noise [22]. The former is normally of high or very high intensity, short duration and is localized both in time and space, while the latter is usually ubiquitous and of moderate or high intensity. A recently proposed candidate for continuous noise indicator is based on Excess Noise Level (ENL), which is the anthropogenic noise on top of the natural background ambient sound [21]. One fundamental difference from other existing indicators, such as sound exposure (SEL) or sound pressure (SPL) levels, which are based on absolute quantities, is that the ENL is, by definition, is a relative indicator. So, ENL depends on the definition of the natural background level, which raises other questions that are to date still unclear (see Section 4).

Due to the inherent quality and extent limitations of acoustic data recordings, for the validation of model data, the objective of this paper is not so much that of providing truthful sound level estimates for the area and period at hand but more that of proposing a methodology that relies on the coupling of a coherent broadband ENL formulation and a simple field calibration method, allowing to correct for model data systemic biases.

Acoustic recordings were performed in June 2018 at three locations to the southwest of Faial-Pico Islands, in the Azores. The quality of the data set as well as recording equipment

limitations are taken into account. For modeling purposes, anthropogenic noise was reduced to shipping drawn from AIS data, and environmental noise was attributed to surface wind only. Data-model comparison allowed introducing spatial weighted field calibration model corrections for an extended area covering four islands, where baseline and ENL fields were estimated. It is therefore expected for the results to provide a basis for ground truth and meaningful policy indicators of ocean noise pollution.

This paper is organized as follows: Section 2 provides the theoretical background of the models and proposed methods as well as a description of the acoustic recordings; Section 3 describes the results obtained using the Faial–Pico data set to generate sound maps for a wider area (central group of islands of the Azores archipelago); Section 4 discusses the results obtained; and finally, conclusions are drawn in Section 5.

2. Materials and Methods

2.1. Environmental Data and Ship Traffic

The Azores archipelago central group is formed by five islands, four of which are shown in Figure 1 along with the bathymetry as extracted from the GEBCO² database [23]. The study area is dominated by deep water with two prominent features: one is the shallow channel between Faial and Pico islands, with a mean depth of only 80 m and the other is an area of shallow banks (<200 m depth) to the southwest of Faial Island, which is a known fishing area. The center box designates the area where the three acoustic recorders (named as CA, IN and MG) were moored.

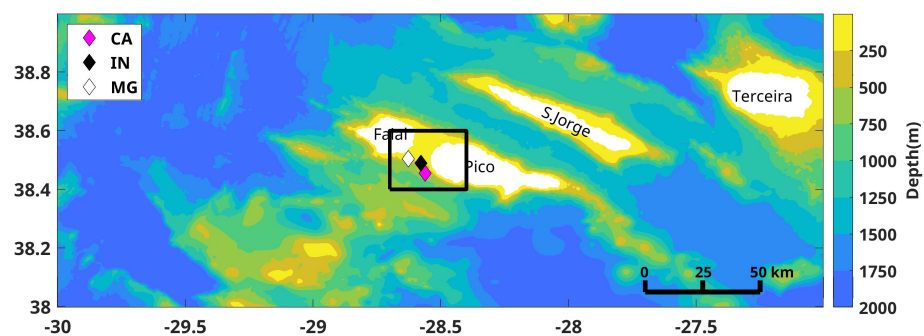


Figure 1. Azores archipelago central group: bathymetry according to GEBCO database [23]. The center box designates the area where the three acoustic recorders (CA, IN and MG) were moored.

Figure 2 shows cumulative plots of temperature, salinity and sound velocity profiles with their mean (in red), taken in point stations across the study area and for the month of June 2018. These data were obtained through numerical modeling with sea surface temperature, sea level and thermistor data assimilation, from the CMEMS-Copernicus Marine Service³ database. The water column shows a typical downward refracting sound velocity profile with a deep sound channel and where the critical depth is not reached.

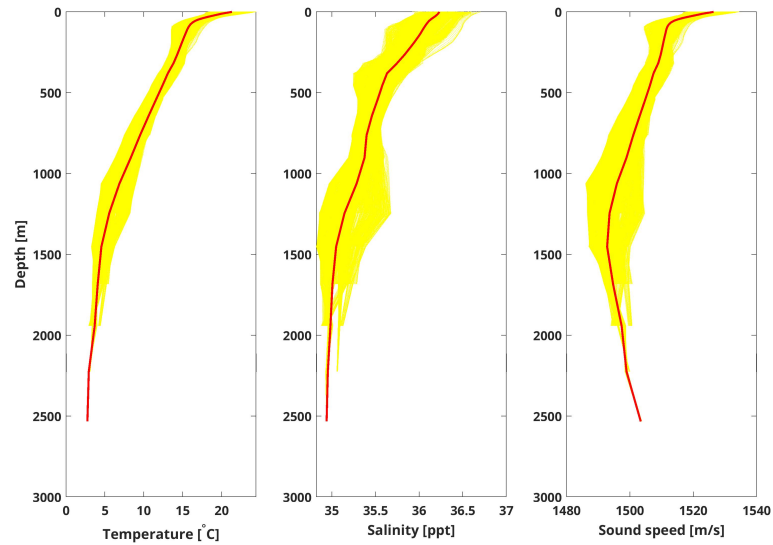


Figure 2. Cumulative temperature, salinity and sound velocity profiles along the study area for the month of June 2018. The mean profiles are shown in red. Source: CMEMS—Copernicus Marine Service.

Figure 3 shows the mean wind speed over the month of June 2018 as predicted by the ECMWF⁴ [24].

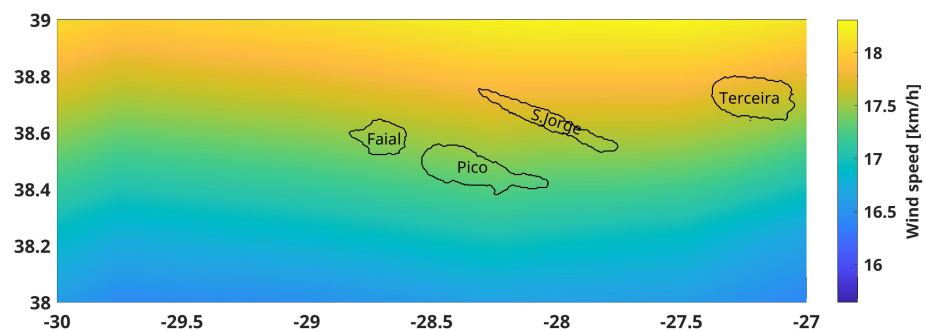


Figure 3. Azores mean wind speed for June 2018. Source: ECMFW [24].

The cumulative ship distribution drawn from AISHub⁵ over the whole month of June 2018 for the study area is given in Figure 4 using logarithm base 10 of ship density evaluated in ship \times hour per arc minute².

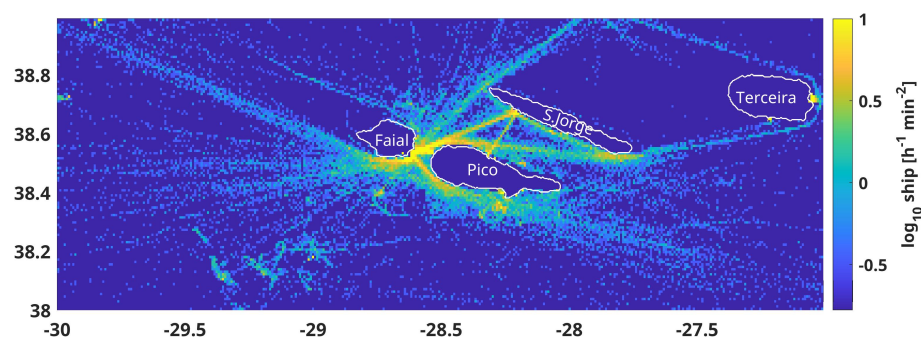


Figure 4. Cumulative ship density for the month of June 2018. Source: AISHub.

2.2. Acoustic Recordings

Acoustic data were recorded with three Ecological Acoustic Recorders (EARs) [25]. These are duty cycle programmable long endurance deep water recorders with an assumed flat sensitivity over the band 20–1000 Hz, operated at a sample rate of 2000 Hz, 16 bit

resolution, 47.5 dB total chain gain and a zero-to-peak voltage at the ADC input of 1.25 Volts. An antialiasing low-pass filter was used to avoid out of band energy spillover, and a high-pass filter set at 20 Hz is used by default to attenuate high-amplitude ocean pressure oscillations. SPL was obtained for 1 s duration Hann-windowed intervals with 50 % overlap using the PAMGuide tool [26]. The PAMGuide is an open source tool running under Matlab® and R which has been widely used and benchmarked ⁶. The three recorders at locations CA, IN and MG (shown in Figure 1) have individual sensitivities of −193.44, −193.14, and −194.17 dB re 1 V/μPa, and they were moored at depths of 484, 200 and 200 m, respectively. Recorders’ position aimed at recording traffic to the west (MG), to the east (CA) and through the channel (IN). Depth was 10 m above the bottom at each chosen location in order to avoid too strong currents and the associated flow noise. For model comparison, the data were averaged in 10 min intervals and summed in 1/3-octave (base 10) bands over the 40–1000 Hz frequency interval. Internal clock drift exists and is on the order of 1.5 s/day, but it has not been measured for that specific deployment, so data validation through individual target tracking is only approximative.

2.3. Ocean Sound Modeling

As mentioned above, and for the frequency band 40–1000 Hz, a two-component model of shipping noise and surface wind generated sound will be assumed. Therefore, the model sound level output L_m will be given by

$$L_m(t, f, \mathbf{r}) = 10 \log_{10} \left[10^{L_S(t, f, \mathbf{r})/10} + 10^{L_w(t, f, \mathbf{r})/10} \right], \tag{1}$$

where L_S is the shipping sound level and L_w is the surface wind generated sound level both in dB, and for time t , frequency f and location \mathbf{r} (latitude, longitude and depth).

2.3.1. Shipping Noise Model

The modeled shipping noise component L_S in (1) is given by

$$L_S(t, f, \mathbf{r}) = 10 \log_{10} \left[\sum_{q=1}^{Q_t} 10^{L_{Hq}(t, f, \mathbf{r}; \mathbf{r}_q)/10} 10^{L_{Sq}(f)/10} \right], \tag{2}$$

due to a shipping distribution of Q_t contributing sources of individual source level $L_{Sq}(f)$ (in dB) propagated from the q -th source with a propagation loss $L_{Hq}(t, f, \mathbf{r}; \mathbf{r}_q)$ (also in dB) between source location \mathbf{r}_q and receiver location \mathbf{r} at time t and frequency f . Note that L_{Hq} is negative, since it represents a power loss along the propagation path. The number of ship sources Q_t , source type and position \mathbf{r}_q are obtained through AISHub (see above). The RANDI model [27], recently updated with the inclusion of uncertainty [28], has been successfully used for determining source level. However, this model was not used in this study since it typically requires additional input information, some of which was missing, potentially leading to a higher uncertainty. Therefore, source level coefficient L_{Sq} was deduced from historical measurements in a lookup table style, according to ship type from McKenna et al. [29], except for sailing vessels whose source level was empirically set to 1% of that of cargos ≈ 20 dB (see [30,31] for details). Source depth for the various ship types was set according to Scrimger and Heitmeyer [32]. Transmission loss is estimated with the Kraken normal mode model [33] using environmental information described in Section 2.1. Specific bottom properties for the area were not available; therefore, a generic bottom composed of one sand covered a 10 m thick sediment layer over a semi-finite hard rock half space was used [13]. Taking into account the mean water depth in the area, the role of the bottom on transmission loss estimation is expected to be minimal.

2.3.2. Surface Wind Sound Model

The term L_w in (1) is the surface wind generated sound level component for a wind speed measured (or predicted) at time t , frequency f and position \mathbf{r} , using the ECMWF

database [24]. The adopted wind generated sound model is that proposed by Kewley et al. [19] that assumes a double mechanism: one for low sea state, and another for high sea state involving the formation of white caps, with a crossing wind speed of about 8 to 10 kn. According to this model, the wind sound term in (1) may be written as

$$L_w(t, f, \mathbf{r}) = 10 \log_{10} \left[10^{L_1(f,v)/10} + 10^{L_2(f,v)/10} \right], \tag{3}$$

where the two parameters L_1 and L_2 are, respectively, given by

$$L_1(f, v) = \alpha(f) + 10 \log_{10} v, \tag{4}$$

$$L_2(f, v) = \beta(f) + 30 \log_{10} v, \tag{5}$$

where α and β are two coefficients obtained from curve fitting on the experimental wind sound spectra, and where v is the scalar wind speed [19]. For the case at hand, this requires resorting to the a priori source level spectra and to the assumed bottom loss curves, whose process is described in [19], and the result is given in Figure 5, where data-drawn curves (continuous lines) are approximated by (3)–(5) (dashed lines), for wind speed (a) and for sound level (b).

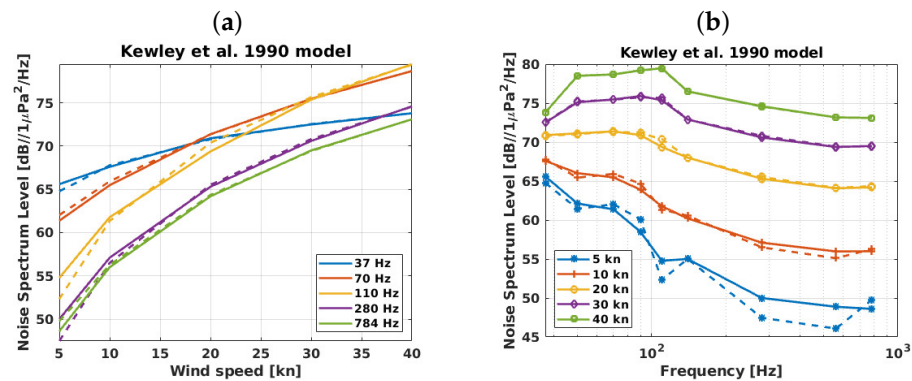


Figure 5. Kewley et al. [19] empirical wind sound model nonlinear least squares fitting of data drawn model (continuous lines) with (3) (dashed lines) for noise level as a function of: wind speed (a) and frequency (b).

Clearly, curve fitting is better for higher wind speeds.

2.4. Simple Field Calibration

Assuming the ocean sound modeling simplifications above, the field calibration process may be schematically represented by the diagram of Figure 6.

The calibration feedback (dashed lines) act on the source level inputs (1) or on the environmental properties inputs (2) to the acoustic model as proposed in [20,21], respectively, or directly onto the modeled field (3), as proposed here. An open possibility is to act simultaneously on several input parameters, but to our knowledge, that has not been attempted to date.

The standard procedure follows to estimate sound maps in 1/3-octave frequency bands (base 10) represented by their center frequencies. With each center frequency, one may associate an SPL empirical distribution deduced from the data observations and another one from the model predictions. In theory, assuming a Gaussian distributed acoustic pressure, SPL should be distributed according to a modified χ^2 with a number of degrees of freedom equal to the number of power bins time-averaged to obtain the SPL estimate. However, when the number of averaged bins is large (say ≥ 30), the corresponding χ^2 distribution tends to a Gaussian distribution via the central limit theorem, so it is fully characterized by its two first moments.

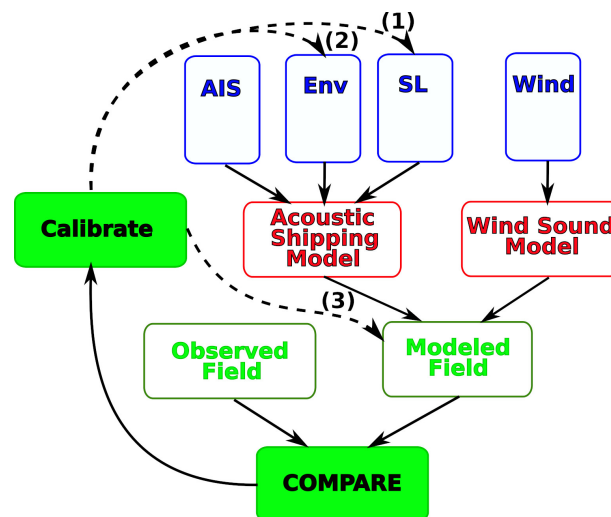


Figure 6. Continuous noise low-frequency field calibration by acting on: (1) the assumed ship source level, (2) environmental properties’ inputs to the acoustic model, or (3) directly on the model distribution output (AIS: Automatic Identification System; Env: environmental information; SL: source level; Wind: wind distribution information).

With that in mind, an ad hoc procedure to allow for data-model fitting that is much simpler and easier to implement than those previously proposed would be to perform a simple variable transformation from the model to the data distribution. The simplest example would be given by a linear transformation in the SPL space such as $Y = AX + B$, where B is the mean shift and A^2 represents the variance coefficient. If $X : \mathcal{N}(m_X, \sigma_X^2)$ represents the model samples, then $Y : \mathcal{N}(m_Y, \sigma_Y^2)$ represents the recorded data samples. It follows that $m_Y = Am_X + B$ and $\sigma_Y^2 = A^2\sigma_X^2$. Knowing (m_X, σ_X^2) and (m_Y, σ_Y^2) at the data recording stations, coefficients A and B can be readily determined. A set of coefficients would be calculated for each frequency band across the spectrum, ending up with a spectral calibration coefficient set of the form $\{A(f_k), B(f_k)\}$ for f_k 1/3-octave band (base 10) center frequencies in the (40–1000) Hz interval. A broadband calibrated estimate may be obtained through a power sum over the full band, which requires descending from the level in dB to power. Working out the $10 \log_{10}$ factor allows to write the field calibration linear transform in power as $P_Y = P_X^A 10^{B/10}$, where P_X and P_Y , are the power counterparts of dB levels X and Y , respectively.

If the recording equipment is calibrated, free of interferences and self-noise, data observations may be trustful. In that case, the proposed simple field calibration may correct model systematic biases with the adjustment of the distribution mean and, in case, data spread misfit by adjusting the model variance. This is obvious for the time and locations where the data were gathered. However, there is no guarantee that the same correction coefficients are still valid out of the recording area and time interval. The domain of validity depends on a number of factors, namely on the origin of the data-model mismatch. As an example, if a systematic frequency-dependent mismatch exists due to an erroneous water column sound speed, the proposed field calibration may prove useful for the whole time, period and area.

2.5. Definition of Excess Noise Level (ENL)

The concept of excess noise level (ENL) aims at determining the “amount” of anthropogenic noise in surplus of the natural ocean sound normally present in the ocean [21]. This requires a measurement (or an estimate) of the sound level normally present in the ocean, which is sometimes also known as the background or baseline ocean sound level. Obtaining an ocean sound measurement free of anthropogenic noise is nowadays practically impossible. There were attempts to obtain such estimates by reprocessing old data records

obtained 50 or more years ago in exceptionally quiet places or particular environmental conditions with unclear success [34–36].

The adopted definition for ENL is logically given as the difference in dB between the measured and the baseline SPL at any given point in time t , frequency f and space \mathbf{r} , which is expressed as

$$L_E(t, f, \mathbf{r}) = L_T(t, f, \mathbf{r}) - L_b(t, f, \mathbf{r}), \tag{6}$$

where L_E is the ENL, L_T is the total sound level, and L_b is the baseline ocean sound level without anthropogenic pressures. All quantities are in dB. The total sound field will be obtained either directly as the measured SPL or as the modeled sound level L_m given in (1). Using power pressure quantities P such that for any SPL L in dB, we have $L = 10 \log_{10} P$, we may rewrite (6) as

$$\begin{aligned} L_E(t, f, \mathbf{r}) &= 10 \log_{10} \frac{P_T(t, f, \mathbf{r})}{P_b(t, f, \mathbf{r})}, \\ &= 10 \log_{10} \left[1 + \frac{P_s(t, f, \mathbf{r})}{P_w(t, f, \mathbf{r})} \right], \end{aligned} \tag{7}$$

where the low-frequency band assumption allows considering the total power field $P_T = P_s + P_w$, with P_s being the shipping noise and P_w being the wind sound power, and that the baseline field $P_b = P_w$. Under these assumptions, the instantaneous ENL given by (7) will be always ≥ 0 . While the instantaneous ENL aims at determining excess noise taking into account the modeled conditions at a given time and location, an alternative would be to define the baseline level as a mean over time, in which case $P_w(t, f, \mathbf{r})$ in (7) will be replaced by the mean value over time $\bar{P}_w(f, \mathbf{r})$.

2.6. The Broadband Case

Farcas et al. [21] proposed a definition for the broadband ENL where full field and baseline levels' difference are averaged over the band as (using the notation above)

$$L_E(t, \mathbf{r}) = 10 \log_{10} \left[\sum_{k=1}^K 10^{[L_T(t, f_k, \mathbf{r}) - L_b(t, f_k, \mathbf{r})]/10} \right] - 10 \log_{10} K, \tag{8}$$

where K is the number of 1/3-octave frequency bands (base 10). The second term in (8) is, according to the authors, a correction term to adjust for zero broadband excess when no shipping noise is present⁷. An alternative way to write (8) is given by

$$L_E(t, \mathbf{r}) = 10 \log_{10} \left[\frac{1}{K} \sum_{k=1}^K \frac{P_T(t, f_k, \mathbf{r})}{P_b(t, f_k, \mathbf{r})} \right], \tag{9}$$

where it is clear that this ENL definition amounts to the average of the ratio of total power to the baseline power which is, in this case, the wind generated sound power P_w .

The dependence on the correction term may be avoided if, instead of the average of the ratio, we use the ratio of the average. In that case, the proposed alternative definition for ENL would be

$$L_E(t, \mathbf{r}) = 10 \log_{10} \left[\frac{\sum_{k=1}^K P_T(t, f_k, \mathbf{r})}{\sum_{k=1}^K P_b(t, f_k, \mathbf{r})} \right], \tag{10}$$

where the $1/K$ coefficient disappears in the ratio. The summation of power over the band that appears in the numerator and denominator of this ratio represents, according to the Parseval theorem, the total field energy and the baseline energy. Energy is the meaningful, and thus the preferred, quantity for the definition of excess noise as an indicator of harm to marine life.

3. Results

This section presents and explains how results were obtained, while their detailed discussion is deferred to the next section.

3.1. Faial-Pico Acoustic Data Set

It is relatively usual to analyze the statistical behavior of an ocean sound data set through its spectral probability density. These are shown in Figure 7 for the received data at the three locations CA, IN and MG in plots (a) to (c), respectively. For each 1 Hz frequency bin, the power spectrum samples obtained on 1 s duration intervals over the whole month with 50% time overlap but no averaging are sorted on 1 dB slots. The color scale denotes a normalized sample count in order to yield an elementary probability estimate for each sound pressure level across the frequency band.

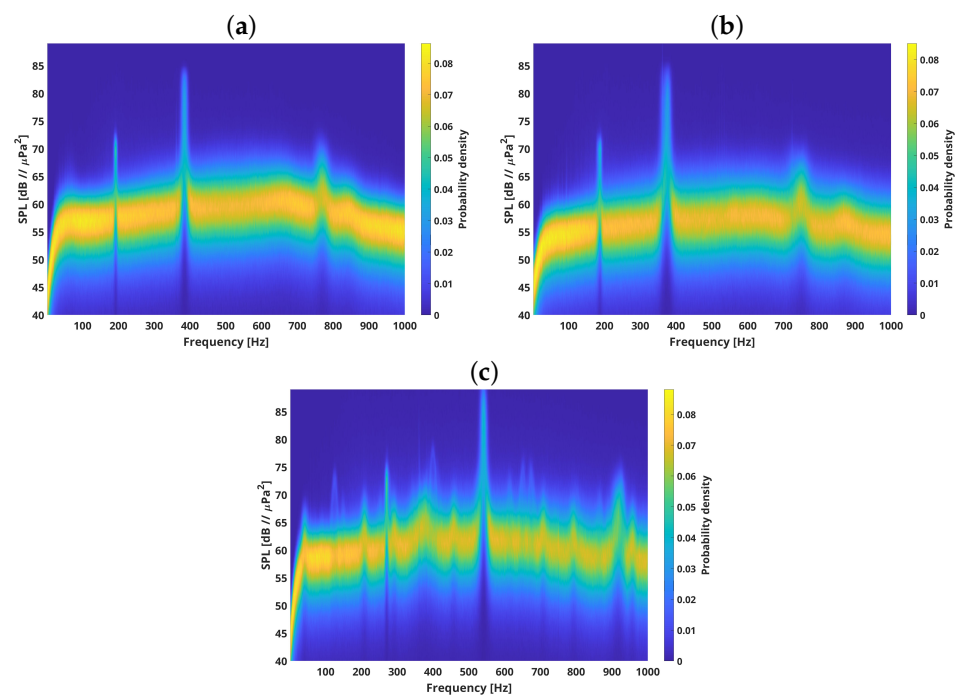


Figure 7. Spectral power distribution with 1 s, 50% overlap time slots between 14:00 and 20:00 UTC in June 2018 for recorders at sites CA (a), IN (b) and MG (c).

Large spurious peaks corrupt the data in some narrow frequency bands for CA and IN (plots (a) and (b)) and possibly over several frequencies for MG (plot (c)). These peaks are hardware related, which is possibly due to a defecting amplifier gain. The data gathered in the frequency bands where these oscillations occur are targeted as self-noise and therefore unusable for field calibration; these should be excluded during processing.

3.2. Experimental and Modeled Data

Figure 8 shows histograms through time of the experimental data (red), shipping-surface wind sound modeled data (blue) and spatial weighted calibrated model data (green) for the CA recording location at the 1/3-octave (base 10) frequency bands between 40 and 1000 Hz. The broadband distribution (bottom right plot) is also shown. Similar results were obtained for locations IN and MG (not shown). In order to mitigate the impact of the data quality impairments found in the previous section, the frequency bands containing the two highest peaks on each plot of Figure 7 were filtered out, according to Table 1. The field calibrated distributions (in green) were obtained with the proposed method (see Section 2.4).

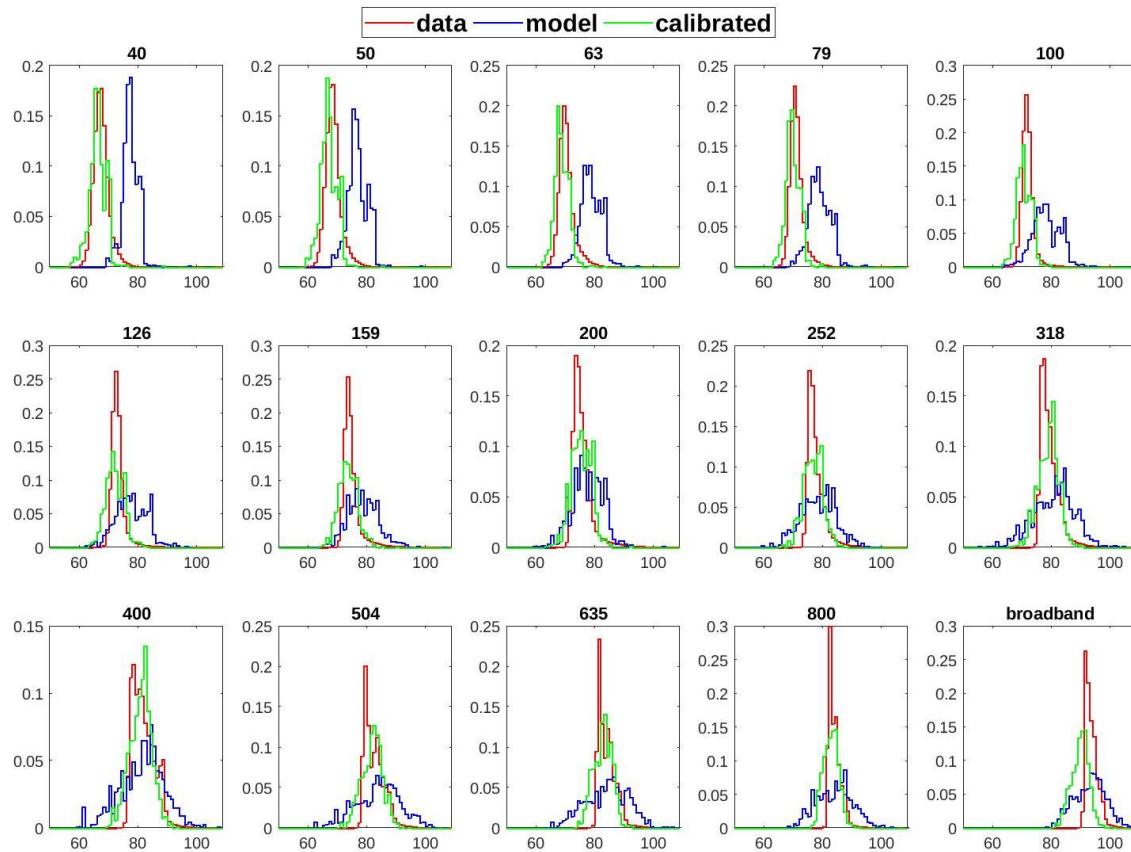


Figure 8. Empirical SPL histograms for 1/3-octave bands (base 10 center frequencies (Hz), and broadband—bottom right) between 40 and 1000 Hz, using 1 s time slots with 50% overlap, between 14:00 and 20:00 UTC in June 2018 for recorder location CA at 484 m depth: recorded data (red), shipping and wind model generated data (blue) and spatial weighted calibrated data (green) (Axes: probability density (y) in 1 dB re μPa , SPL bins (x)).

Table 1. Recorder’s self-noise filtered bands.

Recorder Sites	Bands (Hz)
CA	[188–197], [374–393]
IN	[184–192], [357–387]
MG	[267–274], [528–553]

In this method, the adjusting coefficients $\{A, B\}$ for each location were drawn from a distribution that merges time samples from all three locations CA, IN and MG. This allows including all the observed data in the calibration method which is expected to be more spatially robust than by using individual sensors. In return, the calibrated distributions are not exactly matched (in mean and variance) to the data in each frequency band for each sensor data set. This is illustrated, for the case of CA, in Figure 8, as a slight mismatch between green and red curves. This mismatch can also be noted in the broadband case (bottom right plot), since the calibrated broadband distribution is obtained from the samples summed up over all the frequency bands and not from an adjustment between the broadband model and the data histograms. Overall, for the three locations, the mean absolute error between model and data is in the order of 6.8 dB, and it is reduced to 3.9 dB after calibration.

In order to illustrate ENL estimation, we start by extending the modeling effort to the wide target area producing one sound map every 10 min with a spatial grid resolution of approximately 500 m at 10 m depth. Figure 9 shows the model estimated mean SPL field for each 1/3-octave band (base 10) in (40–1000) Hz and the broadband case for the whole area.

Sound levels are lower for the lower frequency bands, with the broadband case showing the highest level overall. The heavier ship traffic lanes are visible in almost all frequency bands.

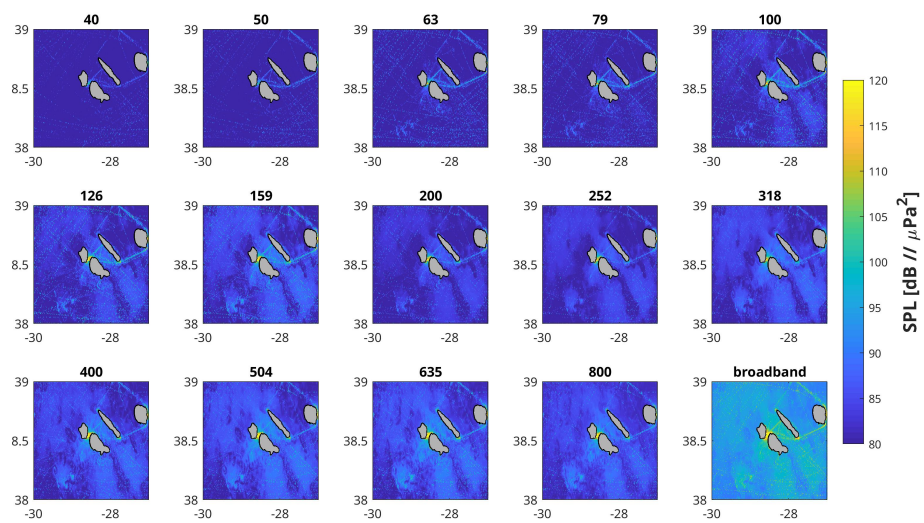


Figure 9. Estimated time mean SPL for the 1/3 octave bands (base 10) center frequencies in (40–1000) Hz and broadband mean using (10) (bottom right plot), at 10 m depth for June 2018 (axes: Latitude (y), Longitude (x) both in decimal arc degrees).

The next step is to compute the ENL using (7) and putting together the whole band using the proposed formulation (10). Figure 10 shows the 95, 75, 50, 25 and 5 percentiles and then the mean broadband instantaneous ENL field at 10 m depth. ENL of up to 35 dB re $1 \mu\text{Pa}^2$ can be estimated in the shallow channel between Faial and Pico Islands only for 5% of the time, with a number of clear outliers present in the mean surface.

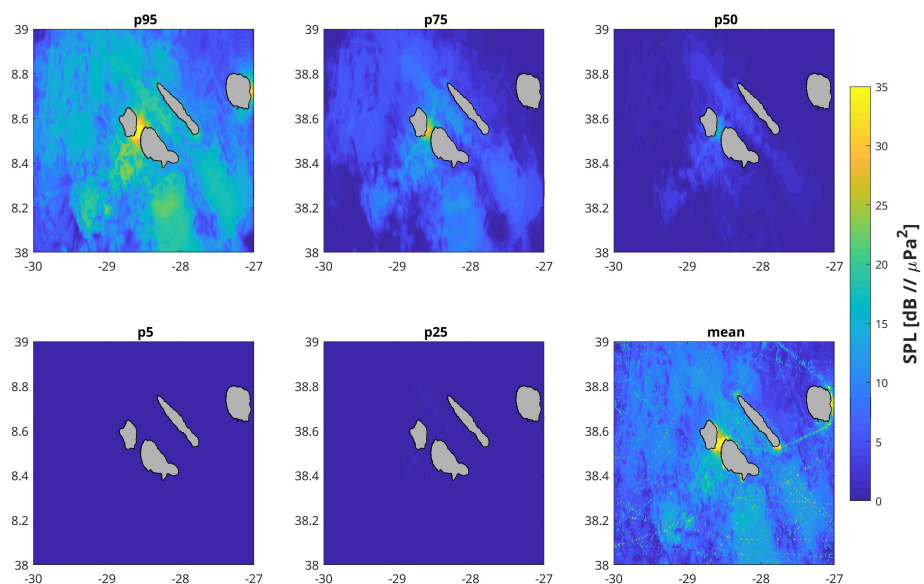


Figure 10. Instantaneous excess noise level (ENL) predicted percentiles and mean over the [40–1000] Hz band at 10 m depth for the Azores central archipelago, in June 2018 with a spatial and time resolution of 500 m and 10 min, respectively (axes: Latitude (y), Longitude (x) both in decimal arc degrees).

3.3. Field Calibration

The simple calibration method outlined in Section 2.4 with the data-dependent modifications set forth in the previous section illustrated in the distributions of Figure 8, was

applied to the modeled data at the recorder locations for verification and then extended to the full study area and time period. Figure 11 shows the predicted ENL statistics for the same parameters as in Figure 10 but using the $\{A, B\}$ field calibration coefficients deduced from the observed data as explained above.

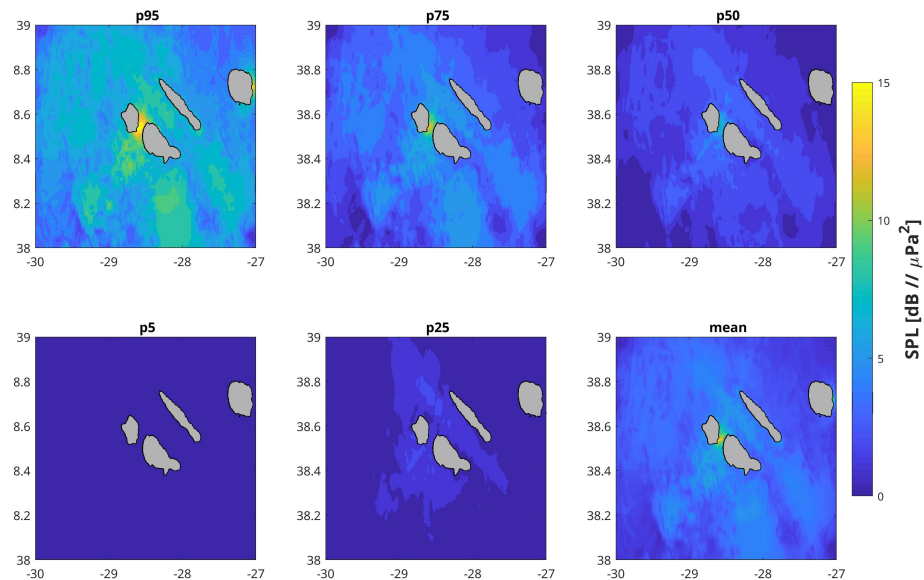


Figure 11. Data-calibrated instantaneous broadband excess noise level (ENL) predicted percentiles and time mean in [40–1000] Hz band at 10 m depth for the wider group of islands, in June 2018 with a spatial and time resolution of 500 m and 10 min, respectively (axes: Latitude (y), Longitude (x) both in decimal arc degrees).

4. Discussion

There are clear high-traffic ship paths around the islands of Faial and Pico as well as to some destinations in S. Jorge Island. Some routes lead northwest to Corvo and Flores, and to Graciosa to the northeast, which are all outside the study area. No traffic zones are clearly identified to the northeast of S. Jorge, around Terceira and to the boundaries of the area. Less traffic does not necessarily mean less noise, especially if these areas are within an acoustic propagation range from intense traffic lanes.

Acoustic data recordings at the three sites to the south of the islands of Faial and Pico are generically consistent with AIS ship traffic density in the area of Figure 4: high noise level is associated with paths of more sustained ship traffic. Figure 7 shows a progressive signal attenuation as frequency decreases below approximately 300 Hz, which is an important band for shipping noise. Additionally, Figure 7 shows that a few tonal frequencies are strongly disrupted by what is believed to be recorders' self-noise. The disturbed frequencies varied from one recorder to the other with peaks up to 30 dB above the mean. These are clearly hardware self-noise related. This legitimately casts doubt on the quality of this particular data set for truthful field calibration. However, the proposed filtering attempts to mitigate this issue without compromising the proposed field calibration and ENL estimation methodology.

Statistical SPL distributions for the 1/3-octave (base 10) bands (Figure 8 red curves) showed relatively narrow density functions with frequency variable mean, self-noise limited low levels (possibly due to the limited number of resolution bits or low gain) and the typical slow drop off queue for higher levels. As previously mentioned, these distributions were obtained after filtering the frequency bands of the main abnormal peaks seen in the spectral probability density of Figure 7.

Histograms for the modeled field, including shipping noise and the surface wind background, were obtained in the same conditions as the data, i.e., for the recorder locations (latitude, longitude and depth) and for the same time frames (14:00–20:00 UTC) (Figure 8

blue curves). In general, the model tends to overestimate the data for the low-frequency bands until 159 Hz while a better model-data fit is obtained for frequencies above. In some cases, the model data distribution is multimodal, which is also found in the observed data, but with a much larger variance. However, no low-level limitation is found in the modeled data. The larger probability peaks found in the data are simply due to the histograms normalization so they can be assimilated to probability density functions with a unit surface. These differences across the spectrum were used as the basis for the proposed field calibration method for the wider area as applied in a “not so good” real data recording.

Modeling is extended to the wider area and for the whole month, as shown in Figure 9. To make a fair comparison, the same color scale is used for all frequency bands. As expected, levels are lower for the lower bands and increase with frequency. Noise peaks up over 120 dB in the channel between Faial and Pico and out of the port of Terceira. Several ship routes are clearly highlighted between Faial-Pico to S. Jorge and Terceira Islands as well as joining other islands. Acoustic SPL peaks scattering from these routes can be seen to the southeast of Faial-Pico-S.Jorge and the shallow banks to the southwest, which is possibly due to the already mentioned fishing activity in the area. The wind model is then used as a baseline for computing the instantaneous ENL using a definition (7) in its broadband form using (10) as shown in Figure 10. Statistical instantaneous ENL analysis through percentiles shows ENL of 15 to 25 dB in extended regions away from the islands but only 5% of the time. ENL progressively reduces down to 10 and 5 dB for percentiles 75 and 50, respectively. Percentiles 5 and 25 are almost flat at a level of only a few dB. This view is consistent with the mean instantaneous ENL broadband plot (bottom right plot).

The calibration process tends to approach the model to the data, imposing lower mean levels in the lower frequency bands and narrower distributions (smaller variances), as shown in Figure 8 (green). The filtering of the self-noise frequency bands and the spatial weighting of the data sets of the three recorders solved those biases, although the tendency of reduced mean levels and variances is still clear in the percentile plots of Figure 11 of the calibrated field when compared to the non-calibrated of Figure 10. For most of the time (p95 and p75), surfaces are flat at only a few dB ENL, while there are a few high peaks reaching over 15 dB at the usual locations and only for small time periods (5 and 25% of the month). Comparison of Figures 10 and 11, before and after calibration, shows an overall ENL mean decrease of approximately 8 dB re 1 μ Pa. The validation of the calibration process is an extremely challenging task due to the lack of observations both in time and space, especially to the east and northeast of Pico Island, although we believe that the proposed calibration methodology provides a balanced adjustment for systematic modeling errors coherent with patterns of the study area. If the same exercise was to be performed in another period of the year, the modeled field would adapt to the then-shipping and wind distributions, and we speculate that a similar adjustment of the model to the data field would be obtained.

5. Conclusions

The Azores is an important habitat for cetaceans [37], but it is also a crossroad of several long-haul shipping routes, and a significant part of its economy is based on marine traffic around and between islands (ferries, leisure, small cargo and fishing). Marine traffic produces ocean noise that impacts on marine species. The Azores is also challenging for acoustic monitoring because it is a vast deep ocean area with a few islands for supporting permanent monitoring buoys or platforms. The goal of this work was twofold: provide evidence for the methodology of broadband ENL estimation as the basis for a continuous noise indicator, and propose a simple field calibration method to extend data collected on three recorders located in a small area during 6 h a day to a wider ocean area for the whole month of June 2018.

It is extremely difficult to properly validate the results obtained without adequate spatial and temporal direct sampling. However, the proposed broadband ENL formulation appears to provide an adequate correlation with the known marine traffic activity in the wider area. More surprising were the vast areas of high ENL to the southeast of the central

islands due to acoustic propagation from the shipping to and from Terceira. However, these only occur for a small portion of the time in the month considered. An attempt for calibrating model predictions in the wide area using field data at a single location induced an overall ENL reduction in the wider area, which is in line with the direct observations of where and when these were performed. Excess levels seem to be relatively low for the considered area and for most of the time during the study period. The authors acknowledge that the calibrated area might be too vast for such a spatially localized small number of observations. The availability of a dedicated tool for determining field calibration spatial coverage with some degree of confidence is lacking.

Author Contributions: Conceptualization, S.M.J.; methodology, S.M.J. and C.S.; software, S.M.J. and C.S.; formal analysis, S.M.J.; investigation, M.R. and I.C.; resources, C.S. and I.C.; data curation, M.R. and F.Z.; writing—original draft preparation, S.M.J. and M.R.; writing—review and editing, M.R., I.C. and M.A.S.; visualization, R.D.; supervision, M.A.S.; funding acquisition, M.R. and M.A.S. All authors have read and agreed to the published version of the manuscript.

Funding: This document contains results of the research performed under project JONAS (grant EAPA 52-2018) funded under the INTERREG Atlantic program of the European Union. Collection of acoustic data was funded by the Portuguese Science & Technology Foundation (FCT) through research project AWARENESS-PTDC/BIA-BMA/30514/2017 (FEDER, COMPETE, QREN, POPH, ESF, PORLisboa, Portuguese Ministry for Science and Education), M.R. was funded by DRCT (grant M3.1.a/F/028/2015), I.C. by FCT-IP Project (grant UIDP/05634/2020), and M.A.S. by AZORES 2020, through the EU Fund 01-0145-FEDER-000140 “MarAZ Researchers: Consolidate a body of researchers in Marine Sciences in the Azores”, and Okeanos by FCT (grant UIDB/05634/2020).

Institutional Review Board Statement: Not applicable.

Informed Consent Statement: Not applicable.

Data Availability Statement: Data not publicly available.

Acknowledgments: We thank Marc Lammers and Sérgio Gomes for technical support with the EARs.

Conflicts of Interest: The authors declare no conflicts of interest.

Notes

- 1 By the Global Ocean Observation System (GOOS)
- 2 General Bathymetric Chart of the Oceans, <https://www.gebco.net>, accessed on 30 November 2021
- 3 www.copernicus.eu, accessed on 30 December 2021
- 4 European Centre for Medium-Range Weather Forecasts, www.ecmwf.int, accessed on 30 January 2022
- 5 Ship Automatic Identification System data exchange, www.aishub.net, accessed on 30 January 2021
- 6 Including Matlab® and R codes supplementary information. <https://doi.org/10.1111/2041-210X.12330>, accessed on 30 January 2021
- 7 After contacting the authors, a typographical error was corrected in the paper Equation (1) to obtain (8).

References

1. Jensen, F.; Kuperman, W.; Porter, M.; Schmidt, H. *Computational Ocean Acoustics*; AIP Series in Modern Acoustics and Signal Processing; Springer: New York, NY, USA, 1994.
2. Hildebrand, J. Anthropogenic and natural sources of ambient noise in the ocean. *Mar. Ecol. Prog. Ser.* **2009**, *395*, 5–20. <https://doi.org/10.3354/meps08353>.
3. Hawkins, A.; Popper, A. Assessing the impact of underwater sounds on fishes and other forms of marine life. *Acoust. Today* **2014**, *10*, 30–41.
4. Williams, R.; Wright, A.; Ashe, E.; Blight, L.; Brintjes, R.; Canessa, R.; Clark, C.; Cullis-Suzuki, S.; Dakin, D.; Erbe, C.; et al. Impacts of anthropogenic noise on marine life: Publication patterns, new discoveries, and future directions in research and management. *Ocean Coast. Manag.* **2015**, *115*, 17–24. <https://doi.org/10.1016/j.ocecoaman.2015.05.021>.
5. Erbe, C.; Marley, S.A.; Schoeman, R.P.; Smith, J.N.; Trigg, L.E.; Embling, C.B. The Effects of Ship Noise on Marine Mammals—A Review. *Front. Mar. Sci.* **2019**, *6*, 606. <https://doi.org/10.3389/fmars.2019.00606>.
6. Duarte, C.M.; Chapuis, L.; Collin, S.P.; Costa, D.P.; Devassy, R.P.; Eguiluz, V.M.; Erbe, C.; Gordon, T.A.C.; Halpern, B.S.; Harding, H.R.; et al. The soundscape of the Anthropocene ocean. *Science* **2021**, *371*, eaba4658. <https://doi.org/10.1126/science.aba4658>.
7. Knudsen, W.; Alford, R.; Emling, J.W. Underwater Ambient Noise. *J. Mar. Res.* **1948**, *7*, 410–429.

8. Urick, R.J.; Pryce, A. *A Summary of Underwater Acoustic Data , Part V, Background Noise*; Technical Report AD/05841; Office of Naval Research: Arlington, VA, USA, 1954.
9. Wenz, G.M. Acoustic Ambient Noise in the Ocean: Spectra and Sources. *J. Acoust. Soc. Am.* **1962**, *34*, 1936–1956. <https://doi.org/10.1121/1.1909155>.
10. Van Oostveen, M.; Barbé, D.; Kwakkel, J. *OSPAR Candidate Indicator Ambient Underwater Sound*; Technical Report BH2849WATRP2003261655; OSPAR: London, UK, 2020.
11. Sirovic, A.; Evans, K.; Garcia-Soto, C.; Hildebrand, J.; Jesus, S.; Miller, J. Trends in inputs of anthropogenic noise into the marine environment. In *World Ocean Assessment II*; United Nations: New York, NY, USA, 2021; Volume 2, pp. 297–320.
12. Colin, M.; Ainslie, M.; Binnerts, B.; de Jong, C.; Karasalo, I.; Ostberg, M.; Sertlek, H.O.; Folegot, T.; Clorennec, D. Definition and results of test cases for shipping sound maps. In Proceedings of the IEEE/MTS Oceans’15, Genova, Italy, 18–21 May 2015.
13. Soares, C.; Zabel, F.; Jesus, S. A shipping noise prediction tool. In Proceedings of the MTS/IEEE Oceans’15, . Genova, Italy, 18–21 May 2015.
14. Skarsoulis, E.; Piperakis, G.; Orfanakis, E.; Papadakis, P. Prediction of shipping noise in the Eastern Mediterranean Sea. In Proceedings of the INTER-NOISE’2016, Hamburg, Germany, 21–24 August 2016; pp. 329–336.
15. Kinda, G.B.; Le Courtois, F.; Stéphan, Y. Ambient noise dynamics in a heavy shipping area. *Mar. Pollut. Bull.* **2017**, *124*, 535–546. <https://doi.org/10.1016/j.marpolbul.2017.07.031>.
16. Urick, R.J. *Principles of Underwater Sound*, 3rd ed.; McGraw-Hill: New York, NY, USA, 1983.
17. Cato, D.H. Ambient sea noise in waters near Australia. *J. Acoust. Soc. Am.* **1976**, *60*, 320–328. <https://doi.org/10.1121/1.381109>.
18. Burgess, A.S.; Kewley, D.J. Wind-generated surface noise source levels in deep water east of Australia. *J. Acoust. Soc. Am.* **1983**, *73*, 201–210. <https://doi.org/10.1121/1.388840>.
19. Kewley, D.J.; Browning, D.G.; Carey, W.M. Low-frequency wind-generated ambient noise source levels. *J. Acoust. Soc. Am.* **1990**, *88*, 1894–1902. <https://doi.org/10.1121/1.400212>.
20. Jesus, S.; Soares, C.; Zabel, F. Shipping noise field calibration via source inversion. In Proceedings of the IEEE MTS/OES Oceans 2017, Aberdeen, UK, 19–22 June 2017.
21. Farcas, A.; Powell, C.F.; Brookes, K.L.; Merchant, N.D. Validated shipping noise maps of the Northeast Atlantic. *Sci. Total Environ.* **2020**, *735*, 139509. <https://doi.org/10.1016/j.scitotenv.2020.139509>.
22. Commission, E. On criteria and methodological standards on good environmental status of marine waters. *Off. J. Eur. Union*; **2010**, *232*, 14–24.
23. Group, G.B.C. The GEBCO_2020 Grid—A Continuous Terrain Model of the Global Oceans and Land. 2020. Medium: Network Common Data Form Version Number: 1 Type: Dataset. Available online: <https://doi.org/10.5285/A29C5465-B138-234D-E053-6C86ABC040B9> (accessed on 30 November 2021).
24. Hersbach, H.; Bell, B.; Berrisford, P.; Biavati, G.; Horányi, A.; Muñoz Sabater, J.; Nicolas, J.; Peubey, C.; Radu, R.; Rozum, I.; et al. *ERA5 Hourly Data on Single Levels from 1979 to Present*; Technical Report Copernicus Climate, Change Service (C3S) Climate Data Store (CDS); European Commission: Brussels, Belgium, 2018. <https://doi.org/10.24381/cds.adbb2d47>.
25. Lammers, M.O.; Brainard, R.E.; Au, W.W.L.; Mooney, T.A.; Wong, K.B. An ecological acoustic recorder (EAR) for long-term monitoring of biological and anthropogenic sounds on coral reefs and other marine habitats. *J. Acoust. Soc. Am.* **2008**, *123*, 1720–1728. <https://doi.org/10.1121/1.2836780>.
26. Merchant, N.; Fristrup, K.; Johnson, M.; Tyack, P.; Witt, M.; Blondel, P.; Parks, S. Measuring acoustic habitats. *Methods Ecol. Evol.* **2015**, *6*, 257–265. <https://doi.org/10.1111/2041-210X.12330>.
27. Breeding, J.E.; Pflug, L.A.; Bradley, M.; Walrod, M.H.; McBride, W. *Research Ambient Noise Directionality (RANDI) 3.1 Physics Description*; Technical Report NRL/FR/7176-95-9628; Naval Research Laboratory, Stennis Space Center: Hancock, MI, USA, 1996.
28. MacGillivray, A.; de Jong, C. A Reference Spectrum Model for Estimating Source Levels of Marine Shipping Based on Automated Identification System Data. *J. Mar. Sci. Eng.* **2021**, *9*, 369. <https://doi.org/10.3390/jmse9040369>.
29. McKenna, M.; Ross, D.; Wiggins, S.; Hildebrand, J. Underwater radiated noise from modern merchant ships. *J. Acoust. Soc. Am.* **2012**, *131*, 92–103.
30. Soares, C.; Duarte, R.J.; Silva, M.A.; Romagosa, M.; Jesus, S.M. Shipping noise in the Azores: A threat to the Faial-Pico cetacean community? *Proc. Mtgs. Acoust.* **2020**, *40*, 070012. <https://doi.org/10.1121/2.0001313>.
31. Soares, C.; Duarte, R.; Zabel, F.; Silva, M.A.; Jesus, S.M. Shipping noise predictions from AIS in the Faial-Pico area, Azores archipelago. In *Global Oceans 2020: Singapore—U.S. Gulf Coast*; IEEE: Biloxi, MS, USA, 2020; pp. 1–6. <https://doi.org/10.1109/IEEECONF38699.2020.9389442>.
32. Scrimger, P.; Heitmeyer, R.M. Acoustic source-level measurements for a variety of merchant ships. *J. Acoust. Soc. Am.* **1991**, *89*, 691–699. <https://doi.org/10.1121/1.1894628>.
33. Porter, M. *The KRAKEN Normal Mode Program*; Number SM-245; Tex.Organization, Saclant Undersea Research Centre: La Spezia, Italy, 1991.
34. Andrew, R.; Howe, B.; Mercer, J.; Dzieciuch, M. Ocean ambient sounds: Comparing the 1960’s with the 1990’s for a receiver off the California coast. *ARLO* **2002**, Issue 3, 65–70.
35. Gaul, R.D.; Knobles, D.P.; Shooter, J.A.; Wittenborn, A.F. Ambient Noise Analysis of Deep-Ocean Measurements in the Northeast Pacific. *IEEE J. Ocean. Eng.* **2007**, *32*, 497–512. <https://doi.org/10.1109/JOE.2007.891885>.

-
36. Reeder, D.B.; Sheffield, E.S.; Mach, S.M. Wind-generated ambient noise in a topographically isolated basin: A pre-industrial era proxy. *J. Acoust. Soc. Am.* **2011**, *129*, 64–73. <https://doi.org/10.1121/1.3514379>.
 37. Silva, M.A.; Prieto, R.; Cascão, I.; Seabra, M.I.; Machete, M.; Baumgartner, M.F.; Santos, R.S. Spatial and temporal distribution of cetaceans in the mid-Atlantic waters around the Azores. *Mar. Biol. Res.* **2014**, *10*, 123–137. <https://doi.org/10.1080/17451000.2013.793814>.